

<https://doi.org/10.22201/igeof.00167169p.2022.61.4.2028>

Intense Geomagnetic Storms in The Maximum Phase of Solar Cycle 24 Observed From a Low-Latitude Ground Station

Juan A. Lazzús^{1,2,*} , Ignacio Salfate¹, Pedro Vega-Jorquera¹

Received: January 29, 2020; accepted: April 8, 2022; published on-line: October 1, 2022.

RESUMEN

Debido a las complejidades de la investigación magnetosférica, la instalación y gestión de nuevas estaciones terrestres magnéticas de acuerdo con los estándares modernos es crucial para monitorear las perturbaciones magnetosféricas y los fenómenos relacionados. En respuesta al desarrollo de nuevas herramientas in situ y conjuntos de datos tomados en tierra que respalden estos estudios, se evaluaron los datos generados por la estación terrestre magnética de baja latitud de La Serena (en las coordenadas geográficas: -29.827 , -71.261 ; y coordenadas magnéticas: -16.55 , 0.17) para describir tormentas geomagnéticas intensas. Esta estación en la ciudad de La Serena (Chile), es dependiente del Laboratorio de Física Espacial y Atmosférica de la Universidad de La Serena (LAFESAT). Con estos datos, estudiamos las cinco tormentas geomagnéticas más intensas ($Dst < -100$ nT) ocurridas durante la fase máxima del ciclo solar 24 (desde 2014 hasta principios de 2016). Los resultados muestran que las variaciones de la componente H de las mediciones de la estación La Serena son consistentes con las variaciones del índice Dst reportadas para cada tormenta analizada, obteniendo valores de coeficiente de correlación de hasta 0.97 para tormentas con $Dst < -200$ nT. Además, nuestros resultados son consistentes con la fuerte influencia que tienen de los sistemas de corriente magnetosférica/ionosférica sobre el componente H durante una intensa tormenta geomagnética.

PALABRAS CLAVE: Observatorio magnético, Componentes del campo geomagnético, Ciclo solar 24, Tormenta geomagnética del Día de San Patricio y Índice Dst.

Editorial responsibility: Marni Pazos

*Corresponding author at jlazzus@userena.cl

¹Departamento de Física, Universidad de La Serena, Casilla 554, La Serena, Chile.

ORCID: <https://orcid.org/0000-0003-1136-3395>

² Instituto de Investigación Multidisciplinario en Ciencias y Tecnología, Universidad de La Serena, Casilla 554, La Serena, Chile.

ABSTRACT

Due to the complexities of magnetospheric research, the installation and management of new magnetic ground stations according to modern standards is crucial for monitoring magnetospheric disturbances and related phenomena. In response to the development of new in situ tools and ground-based data sets that support these studies, data generated by La Serena low-latitude magnetic ground station (at geographic coordinates: -29.827 , -71.261 ; and magnetic coordinates: -16.55 , 0.17) to describe intense geomagnetic storms were evaluated. This station in the city of La Serena (Chile), is supported by the University of La Serena's Laboratory for Space and Atmospheric Physics (LAFE-SAT). With these data, we studied the five most intense geomagnetic storms ($Dst < -100$ nT) occurring during the maximum phase of solar cycle 24 (from 2014 to early 2016). Results show that the H component variations of the La Serena station measurements consistent with the Dst index variations reported for each storm analyzed, obtaining correlation coefficient values of up to 0.97 for storms with $Dst < -200$ nT. Also, our results are consistent with the strong influence of the magnetospheric/ionospheric current systems over the H component during an intense geomagnetic storm.

KEY WORDS: Magnetic Observatory, Geomagnetic field components, Solar cycle 24, St. Patrick's Day geomagnetic storm and Dst index.

INTRODUCTION

Ground-level magnetic field data are crucial for several applications, including monitoring of evolving geomagnetic storms and the space weather conditions (Love, 2008; Matzka *et al.*, 2010; Love & Finn, 2011; Mandaia & Korte, 2011; Onsager, 2012; Love & Chulliat, 2013; Waters *et al.*, 2015).

A geomagnetic storm is the strongest perturbation in the Earth's environment. The general triggering for geomagnetic storms is the magnetic interaction/reconnection between the Earth's magnetosphere and interplanetary magnetic field. These disturbances result in intense currents in the magnetosphere and ionosphere (Ganushkina *et al.*, 2018). The strongest geomagnetic storms occur when coronal mass ejections (CMEs) are emitted toward the Earth, causing a substantial injection of energetic particles drifting around the Earth causing a compression of the magnetosphere (Tsurutani *et al.*, 1988; Gosling *et al.*, 1991; Gopalswamy *et al.*, 2005; Chen, 2011; Joshi *et al.*, 2011; Webb & Howard, 2012), and at the same time an intensification of the currents in the magnetosphere-ionosphere system (Ganushkina *et al.*, 2018). The current systems that can be affected during a geomagnetic storm are: (1) the magnetopause currents shielding earth's dipole and the ring current; (2) the symmetric ring current; (3) the cross-tail current along with the closure currents on the magnetopause; and (4) the partial ring current, which connects the Region 2 field-aligned currents (Ganushkina *et al.*, 2018).

During the storm, the ring current particles which are energized causing a compression of the low-latitude horizontal component of the terrestrial magnetic field and change the magnetospheric ring current during a prolonged time interval (Gonzalez *et al.*, 1994). To quantify the effect of this current, the 1-hour-disturbance storm time (Dst) index is employed to characterize the intensity of the geomagnetic storms (Sugiura, 1964). This index uses the geomagnetic field data from 4 low latitude stations: Kakioka KAK (36.2°N , 140.2°E) in Japan; Honolulu HON (21.3°N , 158.0°W) in Hawaii; San Juan SJG (18.1°N , 66.2°W) in Puerto Rico; and Hermanus HER (34.4°S , 19.2°E) in South Africa. From these stations, the time series of the horizontal (H) component of the geomagnetic field

is obtained by subtracting the background magnetic field and the solar quiet (Sq) variation of the geomagnetic field. Thus, the H component is averaged over these stations and normalized to the geomagnetic equator, as $Dst = \overline{H} / \overline{\cos\theta}$, where θ is geomagnetic latitude and the overbars indicate the arithmetic average over longitude (Sugiura & Kamei, 1991). Additionally, other currents produced in the magnetosphere, such as the field-aligned and auroral currents (associated or not with a geomagnetic storm), cause subauroral geomagnetic disturbances that are used for calculating the 3-hour-planetary geomagnetic disturbance (Kp) index (Bartels *et al.*, 1949; Matzka *et al.*, 2021). This index is provided by 13 subauroral stations for eight three-hourly intervals of the day. Each station is calibrated according to its latitude and reports a K-index itself based on a quasi-logarithmic scale that characterizes the geomagnetic activity at the given location and time compared to a calm day curve. This activity is classified into a scale from 0 to 9 where 0 represents very little geomagnetic activity and 9 is an extreme activity (Matzka *et al.*, 2010; Matzka *et al.*, 2021).

Geomagnetic storms evolve in three phases: (1) the initial phase is an abrupt positive variation in the Dst index, called sudden storm commencement (SSC). An SSC is produced by sudden compression in the magnetosphere caused by an increment of the dynamic pressure of the solar wind. (2) the main phase where the Dst index takes negative values during the injection of energized plasma in the equatorial ring current until it reaches a minimum Dst value; and (3) the recovery phase where Dst values increase until they reach pre-sudden commencement values during the return of the geomagnetic field to normality (Gonzalez *et al.*, 1994; Loewe & Prölss, 1997). During this process, Dst values decrease from close to zero to negative until a minimum Dst value of later increases recovers values closer to zero. According to this minimum value, storms are classified into: weak ($-30 > Dst > -50$ nT, with $0 \leq Kp \leq 5$), moderate ($-50 > Dst > -100$ nT, with $5 < Kp < 7$), and intense ($Dst < -100$ nT, with $7 \leq Kp \leq 9$) categories (Gonzalez *et al.*, 1994; Matzka *et al.*, 2021). Thus, a negative Dst index value indicates increasing intensity of the ring current (Gonzalez *et al.*, 1994; Loewe & Prölss, 1997). This Dst decay is controlled by the ring current and the magnetospheric tail current. During the main phase, the ring current increases its density of O⁺ ions, of ionospheric origin, contributing to the plasma pressure in the inner magnetosphere (Keika *et al.*, 2013; Daglis *et al.*, 1999; Welling *et al.*, 2011). During the recovery phase, particle transport into the ring current slows, allowing various loss processes to reduce ring current particle fluxes to their quiet-time level. The loss mechanisms are more efficient near dawn and dusk (Le, 2013) and explain why the ring current and the ionosphere control the electric fields in the interior of the magnetosphere at dawn and dusk (Bogdanova *et al.*, 2014). These effects are due to the electric fields that appear during dusk near the equatorial ionosphere (Tsurutani *et al.*, 2012). Thus, the ring current becomes the dominant Dst source during intense geomagnetic storms, but during moderate storms, its contribution to Dst is comparable with the tail current's contribution (Kalegaev & Makarenkov, 2008).

Intense storms could represent a latent hazard for space technology systems and human activities on the Earth's surface (Hapgood, 2011; Love & Finn, 2011; Love *et al.*, 2014). To study these events, magnetic ground stations around the world monitor the onset of solar-induced storms and give warnings that help diminish related economic losses (Love & Finn, 2011; Onsager, 2012; Love & Chulliat, 2013). Magnetometer measurements of ground stations at low latitudes are used to monitor the electrodynamics of the ionosphere that control ionospheric plasma distributions during a geomagnetic storm (Kamide *et al.*, 1981; Richmond & Kamide, 1988; Yizengaw *et al.*, 2014; Anderson *et al.*, 2004).

In this contribution, we studied five intense geomagnetic storms during the maximum phase of solar cycle 24 by using ground-level magnetic field data gathered at the La Serena low-latitude magnetic ground station as a response to development of new in situ tools and ground-based data sets that support magnetospheric research.

SOLAR CYCLE 24

Solar activity (such as sunspot area, radio flux, solar flares, CMEs, and other related phenomena) can increase or decrease following an 11-year cycle of activity (Schwabe, 1844). Each solar cycle has unique characteristics; however, solar cycle 24 has exhibited hitherto unusual and unprecedented solar activity (Richardson, 2013; Kamide & Kusano, 2013; Gopalswamy *et al.*, 2014; Pesnell, 2014; Watari, 2017).

Solar cycle 24 (2008–present) (Pesnell, 2014), preceded by the lowest and the longest solar minimum in the last solar cycles (Russell *et al.*, 2010; Richardson, 2013), is the most recently completed solar cycle (Kamide & Kusano, 2013; Gopalswamy *et al.*, 2014; Watari, 2017). The extended minimum from ~2008 to 2010 (Gopalswamy *et al.*, 2014; Lingri *et al.*, 2016) was followed by high activity during a short phase beginning at the end of 2011 (Lingri *et al.*, 2016; Watari, 2017) with an activity peak reached before 2013, as it then decreased and peaked again in 2014 (Gopalswamy *et al.*, 2014; Lingri *et al.*, 2016), registering its maximum activity phase from 2014 to 2015 (Pesnell, 2014). Several authors have speculated that this extraordinarily low minimum has shown unexpected Sun and solar wind conditions compared only with strange states of the Sun occurred in the past, such as Maunder and Dalton minima (Agee *et al.*, 2010; McDonald *et al.*, 2010; Feynman & Ruzmaikin, 2011; Hao & Zhang, 2011; White *et al.*, 2011; Williams & Pesnell, 2011). The Maunder minimum (1645–1715) and Dalton minimum (1790–1820) were periods with extremely low sunspot numbers where the Earth experienced abnormal cooling times (Eddy, 1976; Mauquoy *et al.*, 2002; Owens *et al.*, 2017).

INSTRUMENTS AND DATA

In this study, we used data recorded by a low-latitude magnetic ground station. The La Serena magnetic ground station (SER) in the Villa Juan Soldado sector at the outskirts of La Serena, Chile (see Figure 1), is far from urban settlements. For reference, the geographical coordinates of SER are 29.827° S, 71.261° W, at 28 [masl], with corrected geomagnetic coordinates to -16.55 latitude, 0.17 longitude, and L-value of 1.09. SER is supported by the University of La Serena's Laboratory for Space and Atmospheric Physics (LAFESAT) through the Department of Physics of the University of La Serena (DFULS).

SER records geomagnetic field intensity data in nT units using the X (North) Y (East) Z (Down) coordinate system in both ASCII and CDF formats at 1 sec and 1 min time resolution by using a fluxgate magnetometer from the University of California Los Angeles (UCLA). Figure 2 details this instrumentation (Engebretson & Zesta, 2017). Our study applies to five geomagnetic storms observed from 2014 to early 2016. To describe these storms, the geomagnetic Dst index was obtained from Kyoto's World Data Center for Geomagnetism (WDC) database at 1 h resolution (<http://wdc.kugi.kyoto-u.ac.jp/>).

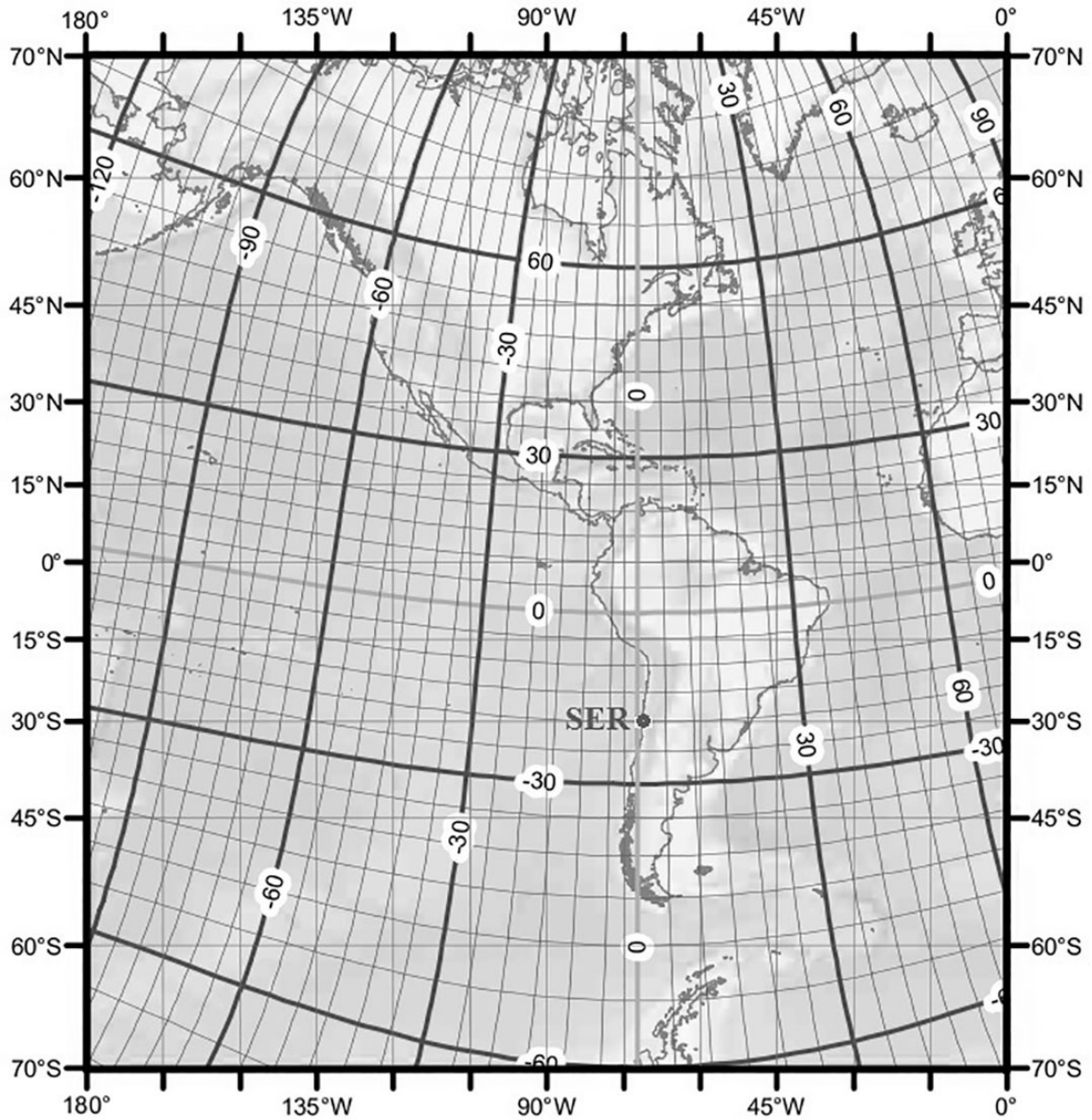


Figure 1. Geographic and magnetic coordinates of SER.

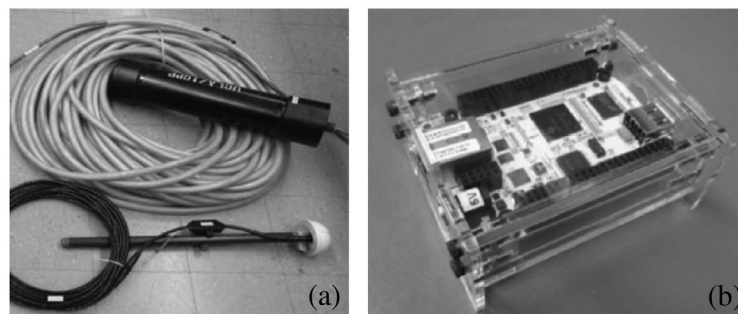


Figure 2. Instruments used by SER. (a) UCLA magnetometer sensor and GPS antenna, and (b) Beaglebone controller/recording system.

Table 1. List of intense geomagnetic storm reported during the maximum phase of solar cycle 24 (in decreasing order).

Code	Start	End	Dst _{min} [nT]	Kp	Type	Solar sources	Reports
I ₁	2015/03/17	2015/03/21	-223	7.7	SC ^a	PH ^c (sheath, MC ^d) CH ^e	(Astafyeva <i>et al.</i> , 2015)
							(Liu <i>et al.</i> , 2015)
							(Baker <i>et al.</i> , 2016)
							(Jacobsen & Andalsvik, 2016)
							(Kalita <i>et al.</i> , 2016)
							(Goldstein <i>et al.</i> , 2016)
							(Hairston <i>et al.</i> , 2016)
							(Nava <i>et al.</i> , 2016)
							(Salinas <i>et al.</i> , 2016)
							(Verkhoglyadova <i>et al.</i> , 2016)
							(Wu <i>et al.</i> , 2016)
							(Yao <i>et al.</i> , 2016)
							(Zakharenkova <i>et al.</i> , 2016)
I ₂	2015/06/22	2015/06/24	-204	7.7	SC	PH (sheath, MC) multiple	(Liu <i>et al.</i> , 2015)
							(Baker <i>et al.</i> , 2016)
							(Gromova <i>et al.</i> , 2016)
							(Reiff <i>et al.</i> , 2016)
							(Le <i>et al.</i> , 2017)
I ₃	2015/12/19	2015/12/22	-155	6.3	SC	Hf (MC)	(Watari, 2017)
							(Watari, 2017)
I ₄	2014/02/18	2014/02/22	-119	6.3	GC ^b	PH (MC) multiple	(Atulkar <i>et al.</i> , 2014)
							(Zakharenkova <i>et al.</i> , 2015)
							(Ghamry <i>et al.</i> , 2016)
							(Durgonics <i>et al.</i> , 2017)
I ₅	2015/12/31	2016/01/02	-110	6.0	SC	PH (MC)	(Berdichevsky <i>et al.</i> , 2016)
							(Watari, 2017)

^aSC: sudden commencement; ^bGC: gradual commencement; ^cPH: partial halo CME; ^dMC: magnetic cloud; ^eCH: coronal hole; ^fH: full halo CME.

COMPARISON OF LOCAL MEASUREMENTS AND GLOBAL INDEXES

We investigate five intense geomagnetic storms ($Dst < -100$ nT, $7 \leq Kp \leq 9$) that occurred during the maximum phases of solar cycle 24. Note that the magnetosphere and solar wind parameters (e.g. IMF and plasma parameters) and other solar sources (e.g. CME) of these storms are not studied here. Thus, we select the most intense events registered between 2014 and early 2016 whose characteristics and sources many authors reported (see, Table 1). This Table summarizes the main characteristics of the selected storms.

To describe these events from ground-level measurements, we employ a graphical description based on: (i) the local records of the XYZ-components of the geomagnetic field taken from SER (<http://magnetometers.bc.edu/>) to obtain horizontal component $H = (X^2 + Y^2)^{1/2}$ and the rates dH/dt ; (ii) the geomagnetic Dst index taken from the WDC database (<http://wdc.kugi.kyoto-u.ac.jp/>); and (iii) the Kp index taken from GFZ Helmholtz Centre Potsdam (<https://www.gfz-potsdam.de/>), and

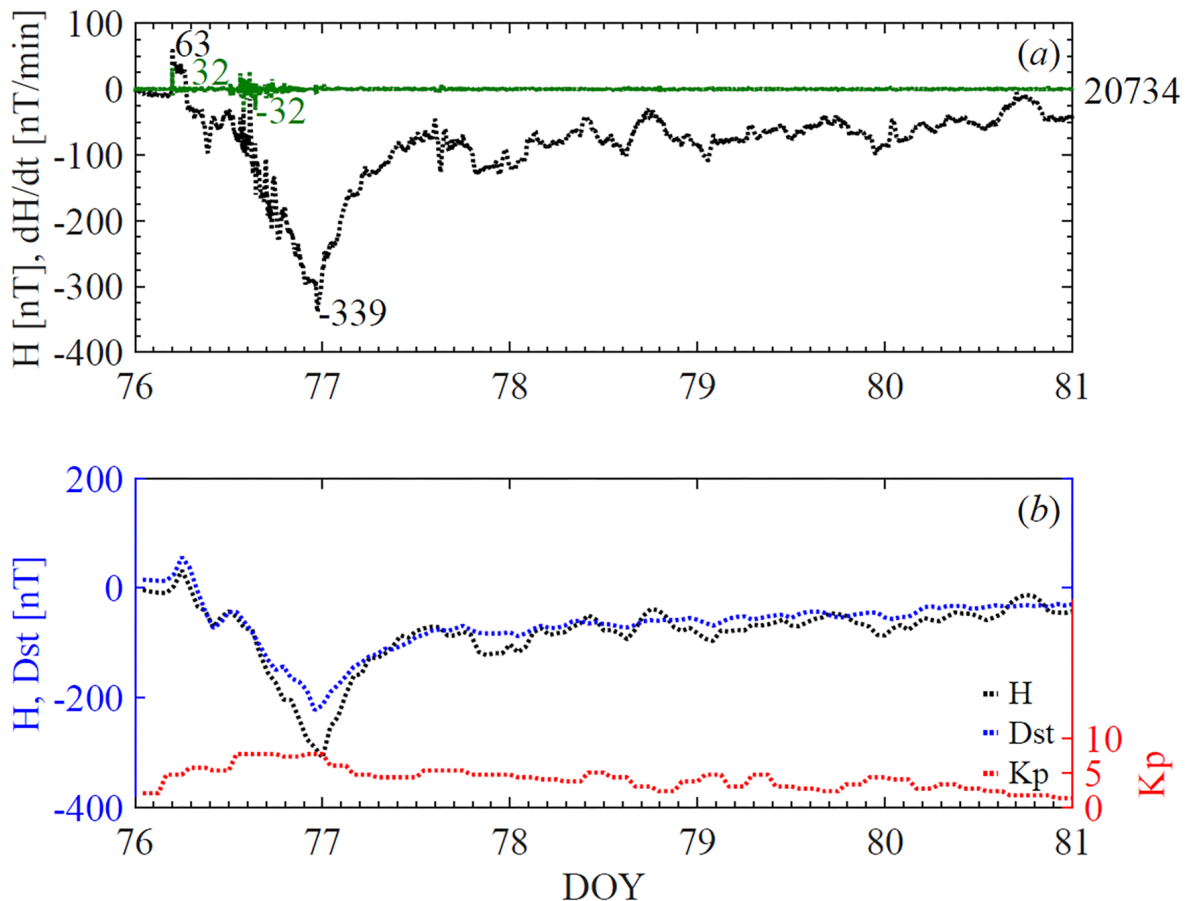


Figure 3. Geomagnetic field variations during the St. Patrick's Day storm (I_1) recorded by SER. (a) H component and rate dH/dt ; (b) comparison of geomagnetic field variations recorded by SER, and the Dst index reported by WDC during this storm. Here, the baseline for the H component was obtained using the method reported by Sugiura & Kamei (1991). The number at the right of the top panel is the reference value obtained by SER. The Kp index in the bottom panel was included to complement the geomagnetic activity due to the storm.

included to complement the geomagnetic activity produced by each storm. In these descriptions, we use universal time (UT) and the day of the year (DOY) to specify the sudden commencement and the phases of each storm.

MARCH 17 (2015) STORM

The March 17–21, 2015 event, called St. Patrick's Day geomagnetic storm, was the most intense storm of solar cycle 24, with a minimum Dst value of -223 nT (Kamide & Kusano, 2015; Wu *et al.*, 2016; Watari, 2017). Figure 3a shows a graphical description of this storm using the H-component of the geomagnetic field recorded by SER at 1 min resolution. Note that in this and the following cases, the baseline for the H component was obtained using the same methodology employed in the derivation of the Dst index (see Sugiura & Kamei, 1991). On March 17 (DOY 76), around 04:45 UT appears the SSC with a 63 nT increase of the H component and a rate $dH/dt=32$ nT/min. Next, the geomagnetic component values fell to a minimum up to $H \approx -200$ nT at 17:00 UT with rates up to $dH/dt=-32$ nT/min. Later, a second storm intensification reached $H=-339$ nT at $\sim 22:00$ UT

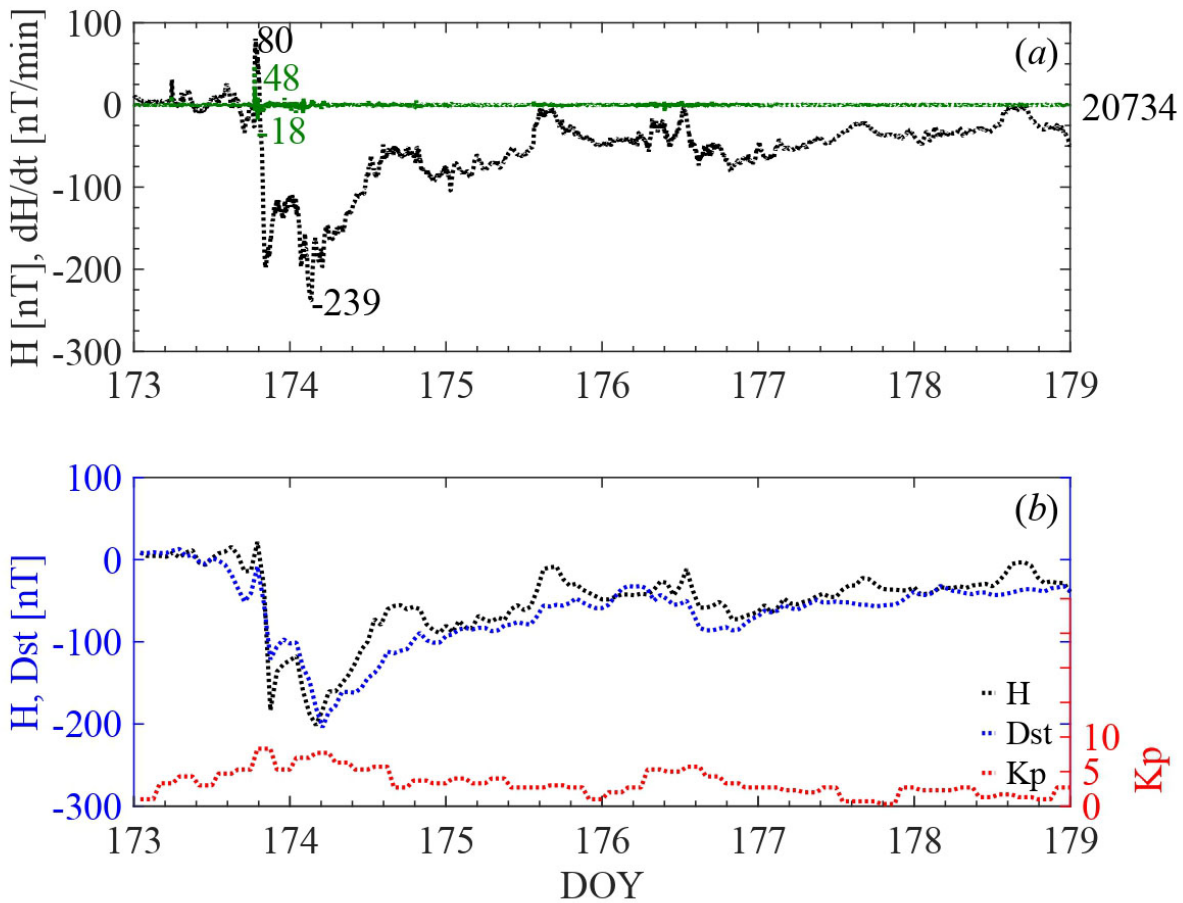


Figure 4. Geomagnetic field variations during the June 22–24, 2015, storm (I2) recorded by SER. The description of this Figure is similar to Fig. 3.

on March 17, and with rates of $dH/dt=10$ nT/min. A few hours later, the geomagnetic component values slowly increased during a recovery phase that lasted several days. Besides, Fig. 3b shows a good correlation between Dst index and the H component for all storms phases.

JUNE 22 (2015) STORM

The geomagnetic storm of June 22–24, 2015, is so far the second most intense event of solar cycle 24 (Le *et al.*, 2017; Piersanti *et al.*, 2017; Watari, 2017). Figure 4 shows its graphical description by using the H-component of the geomagnetic field recorded by SER at 1 min resolution. Fig. 4a displays positive H peak values marking an SSC observed at 06:00 UT on June 22 (DOY 173) with a rate $dH/dt>10$ nT/min. A second SSC was observed around 18:00 UT registering $H=80$ nT and $dH/dt=48$ nT/min. This storm followed a two-step development during its main phase with a first moderate peak at $\sim 20:00$ UT with $H=-190$ nT and $dH/dt=-18$ nT/min; and a second peak of $H=-239$ nT at $\sim 04:00$ UT on June 23 (DOY 174). Next, the recovery phase also unfolded in two-steps observed at $\sim 22:00$ UT on June 23 and at $\sim 14:00$ UT on June 24, both with much rate variation of dH/dt . In addition, Fig. 4b shows the contrast of records of geomagnetic fields measured by

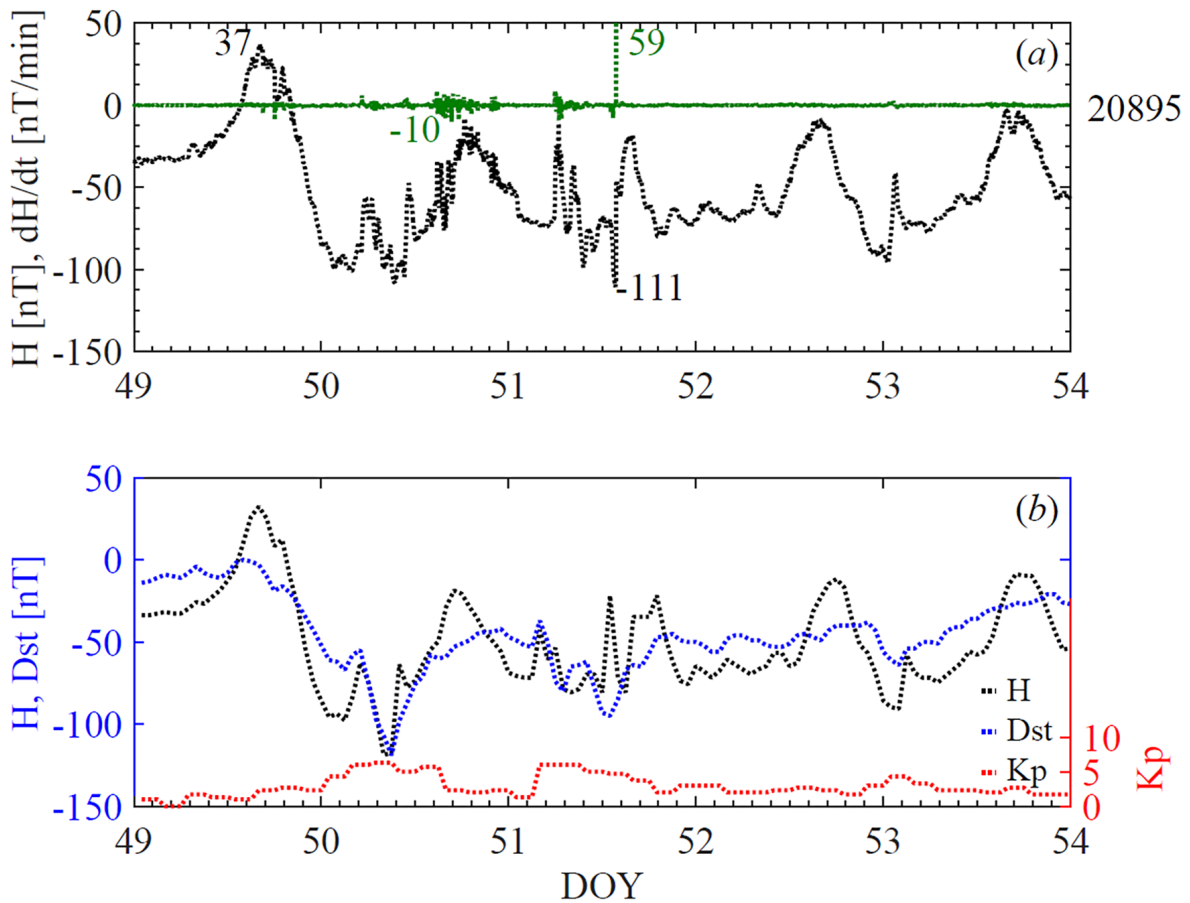


Figure 5. Geomagnetic field variations during the December 19–22, 2015, storm (I3) recorded by SER. The description of this Figure is similar to Fig. 3.

SER and the Dst index reported by WDC. In the Dst data, two minimum value events emerged. One occurred around 05:30 UT on June 23, and the other more powerful event causing a Dst peak of -204 nT on June 24. The storm's main phase lasted about half a day, but its recovery phase took many days. Here, the H component record similar observations as the Dst index.

DECEMBER 19 (2015) STORM

The measured H values by SER (at 1 min resolution) for the December 19–22, 2015, storm and its graphical description appear in Fig. 5a. It shows positive H peak values, corresponding to two SSC at 18:00 UT on December 19 (DOY 353) with $H \approx -110$ nT and $dH/dt = 32$ nT/min; and another at 22:00 UT on December 19 with $H \approx -116$ nT and a rate $dH/dt = 10$ nT/min. Its main phase started during December 20 (DOY 354) and peaked around 22:00 UT that same day, with $H \approx -219$ nT and $dH/dt \approx -12$ nT/min. Then, the geomagnetic component values increased slowly until December 23 (DOY 357). Also, Fig. 5b exhibits the contrast of records between the geomagnetic field measured by SER and the Dst index reported by WDC. Here Dst index shows a minimum of -155 nT at 22:00 UT on December 20 (DOY 254), and similar behavior as H component.

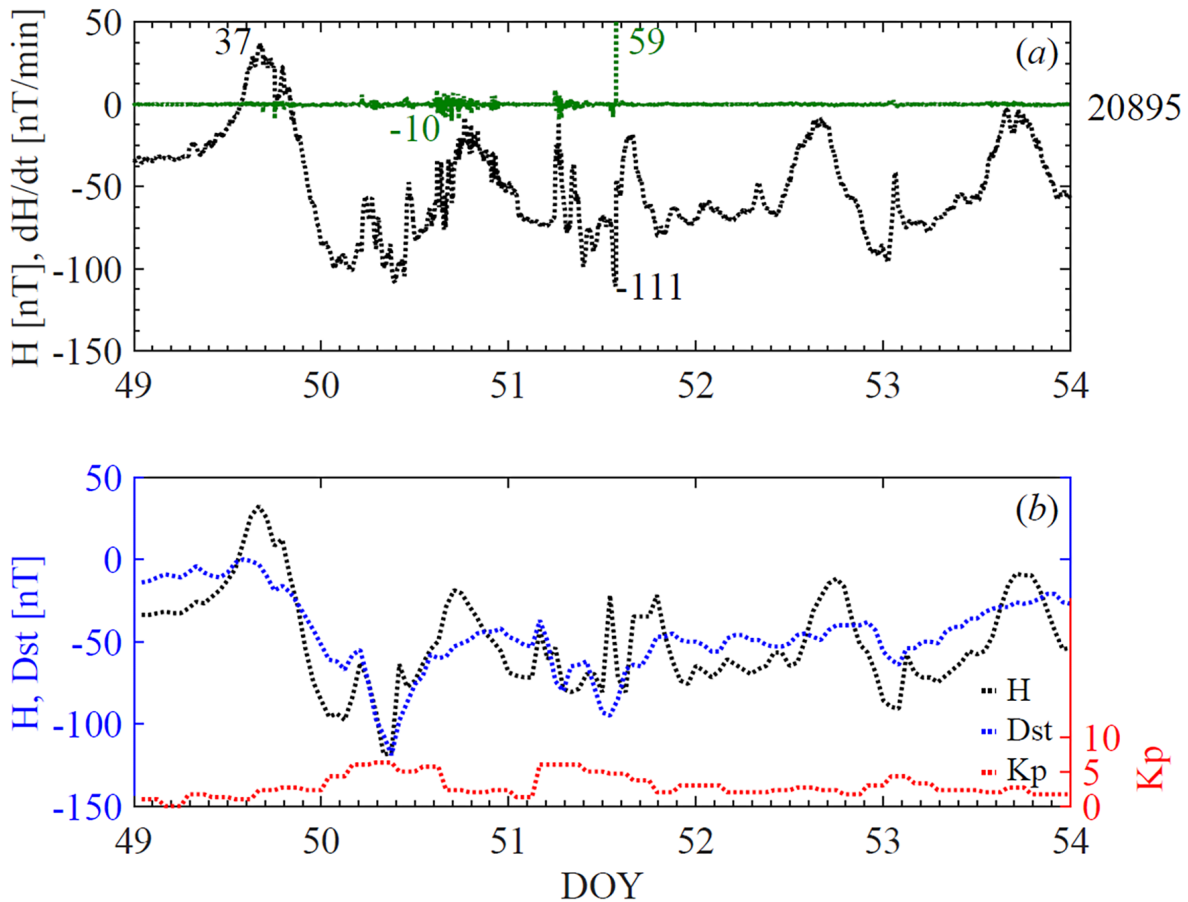


Figure 6. Geomagnetic field variations during the February 18–22, 2014, storm (I4) recorded by SER. The description of this Figure is similar to Fig. 3.

FEBRUARY 18 (2014) STORM

A graphical description of the February 18–22, 2014, storm appears in Figure 6. This Figure details two successive storms that hit the Earth's magnetosphere, recorded by the H component of the geomagnetic field (at 1 min resolution) in SER. Fig. 6a shows the positive values on the H component of the geomagnetic field with amplitude $H=37$ nT at $\sim 14:00$ UT marking the SSC that started the first storm on February 18 (DOY 49). This manifests with a rate $dH/dt \sim 5$ nT/min. The peak of this first event ($H=-109$ nT) was observed at $\sim 09:00$ UT on February 19 (DOY 50) with a rate $dH/dt=6$ nT/min. The second event started $\sim 04:00$ UT on February 20 when this storm's main phase started a two-step development and registered rate $dH/dt=-10$ nT/min. On February 20 (DOY 51), the H component dropped to -111 nT at $\sim 12:30$ UT but recovered rapidly to -25 nT and fell again to -58 nT at $02:00$ UT on February 22. Besides, contrasting these observations with the ones provided for the Dst index from WDC, shows the same behavior as the H component with a minimum $Dst=-119$ nT during the first storm (DOY 50) and another minimum of -95 nT for the second storm on February 20 (DOY 51) as in Fig. 6b.

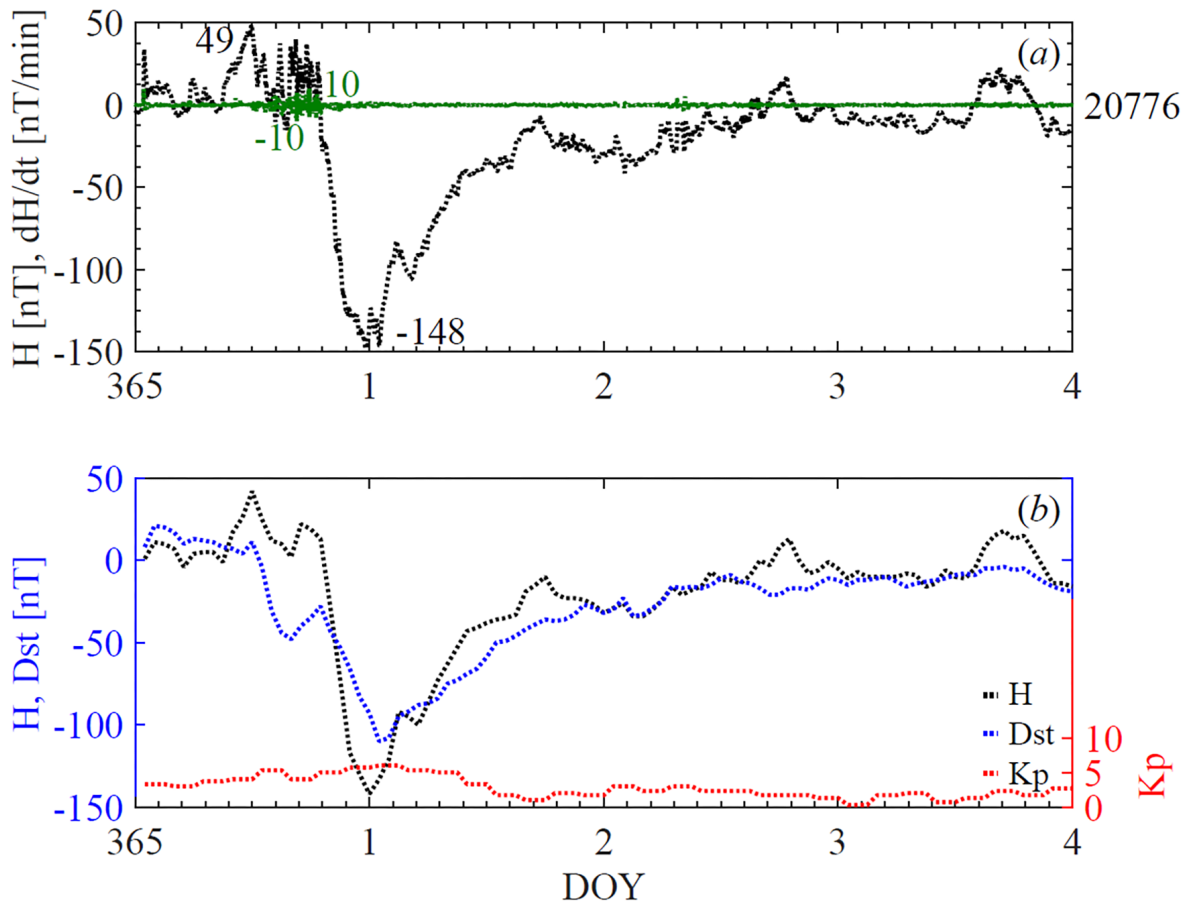


Figure 7. Geomagnetic field variations during the geomagnetic storm on December 12, 2015–January 01, 2016 (15) recorded by SER. The description of this Figure is similar to Fig. 3.

Table 2. Summary of correlation coefficients (R) obtained between Dst index (taken from WDC Kyoto) and H component (recorded by SER) for the phases of each storm studied (columns 3 to 6). In addition, the signs for the difference between their minimum magnitudes, and for its time difference are included in columns 7 and 8, respectively.

Code	Storm	Correlation coefficients between Dst and H				$\Delta = \text{Dst} - \text{H}$	
		R_{initial}	R_{main}	R_{recovery}	R_{storm}	$\Delta_{\text{magnitude}}$	Δ_{time}
I ₁	2015/03/17–2015/03/21	0.970	0.975	0.944	0.951	+	+
I ₂	2015/06/22–2015/06/24	0.957	0.959	0.902	0.902	+	+
I ₃	2015/12/19–2015/12/22	0.838	0.865	0.852	0.855	+	+
I ₄	2014/02/18–2014/02/22	0.917	0.879	0.504	0.717	–	–
I ₅	2015/12/31–2016/01/01	0.808	0.806	0.940	0.860	+	+

DECEMBER 31 (2015) STORM

Figure 7 shows the graphical description of the December 31, 2015–January 02, 2016 storm using the H component of the geomagnetic field recorded by SER at 1 min resolution. In Fig. 7a, successive positive H component values evidence two SSCs measured at ~12:00 UT and ~16:00 UT on December 31 (DOY 365) during the initial phase of this storm. The maximum amplitude of SSC was $H=49$ nT, with a rate $dH/dt \sim 10$ nT/min. The peak of the storm with $H=-148$ nT occurred at ~00:30 UT on January 01, marking the end of its main phase. After this peak, geomagnetic field values increased slowly during its recovery phase. In addition, Fig. 7b shows the H component of the geomagnetic field taken from SER, and the Dst index taken from WDC at 1h resolution. As is observed, a good correlation between Dst index and H component of the geomagnetic field emerges. Here, the SSC peak in the initial phase (DOY 365), and the minimum Dst index value of -110 nT observed at 00:00 UT on January 01 during the main phase are in agreement with those recorded by the H component in SER.

DISCUSSION

The previous section showed that the instrument seems to be working as expected. The SER detected the five geomagnetic storms and showed a good correlation with the Dst index variations reported by WDC. (see Figs. 3 to 7). In terms of H component, the records obtained by SER can characterize all storm phases, such as the higher H values in the initial phase, followed by the dropped ones of the H component during the main phase, and its restitution to normal levels in the recovery phase. Also, the SSC signatures were evidenced with the rates dH/dt , because they are powerful indicators of disturbances in the ring current (Doumbia *et al.*, 2017).

Table 2 shows the correlation coefficient (R) between the hourly Dst index and the geomagnetic field H-component (at 1h resolution) obtained for each storm analyzed (see columns 3 to 6). For total storm disturbance R_{storm} , only storm I₄ shows $R_{\text{storm}} < 0.8$ while all others show R_{storm} from 0.85 to 0.96. When analyzing the R values for the different storm phases, both the initial and main phases present R_{initial} and R_{main} from 0.8 to 0.97, while the recovery phase shows R_{recovery} from 0.5 to 0.94 being the lowest value for storm I₄. In general, the measurements of the H component of the geomagnetic field recorded by SER show minor discrepancies with the storm behavior described by

the Dst index. Note that the Dst index is an average obtained from different stations. The behavior of individual stations is expected to vary with respect to global value, and the local site response is the important one for each region, but also this discrepancy can be associated with phenomena that contribute to the H component variation, such as (1) the magnetopause current, (2) the symmetric ring current, (3) the cross-tail current, and (4) the partial ring current (Maltsev, 2004). To distinguish the action of these magnetospheric currents on the selected storms, we have represented the time at which the minimum Dst value occurs for each storm. Figure 8 shows the graphical representation of the instant of the minimum Dst at UT and magnetic local time (MLT). In this Figure, the Earth is represented from the North Pole as follows: day side-night side, and dawn-dusk sectors, with the UT represented by the inner circle and the MLT by the outer one. To clarify, the MLT in SER at UT noon is 16:00 MLT. As is observed, storms I_1 and I_3 measured the maximum depression of the H component at 18:00 MLT (but on different dates), and as both have an SSC, they developed the initial and main phases in the dusk zone. In the zone between dusk and midnight, storms I_2 and I_5 (at 20:00 and 00:00 MLT, respectively) developed both their initial and main phases, and a few hours

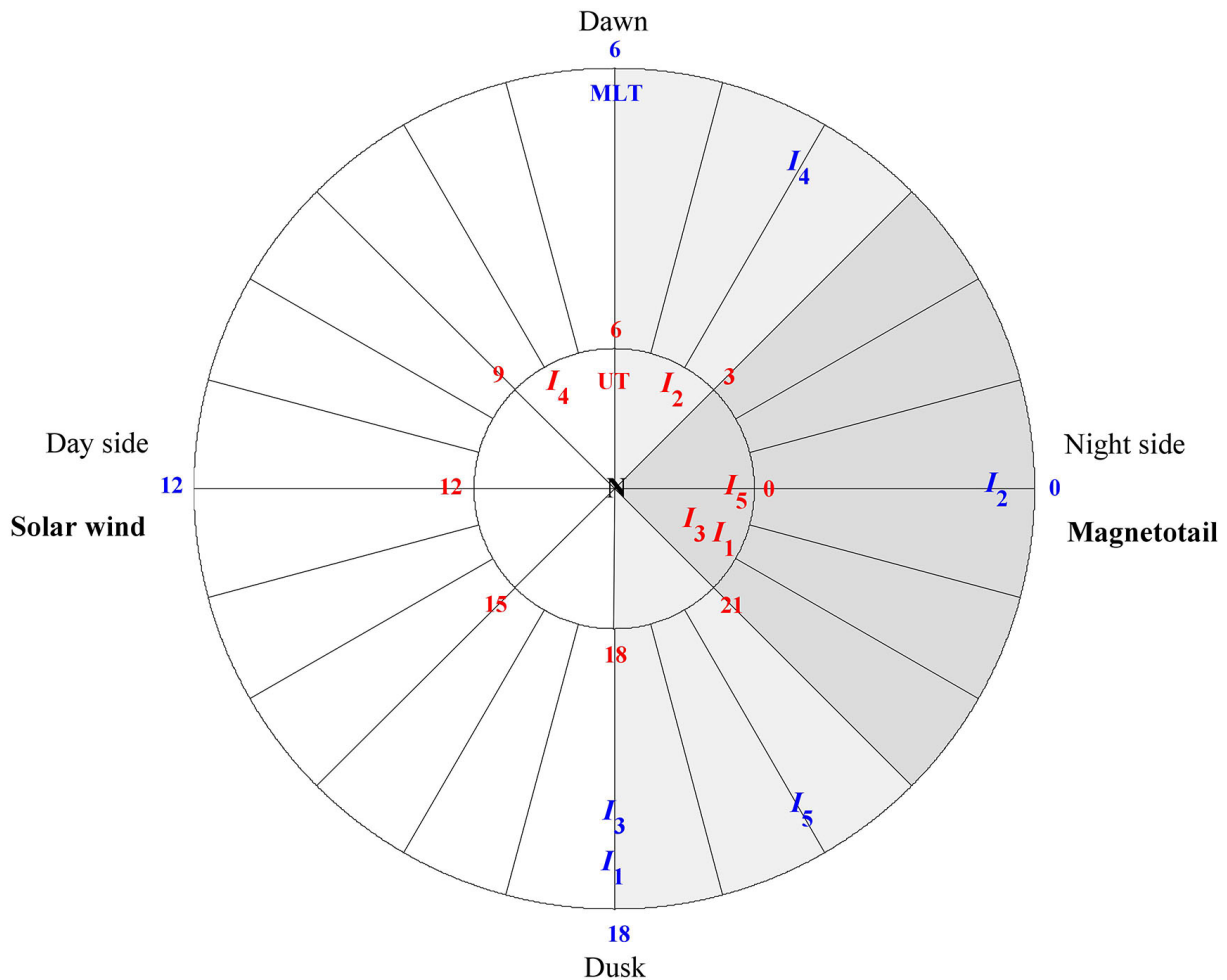


Figure 8. Location of geomagnetic storms studied at the time of their occurrence as a graphical representation of the maximum depression of H component (or the minimum Dst) at UT (the inner circle) and MLT (outer circle). Here, grey sectors represent the night side and white sectors the dayside. Regions of currents are the magnetotail electrojet on the night side, the dawn, the dusk, and the dayside.

later their recovery phase went toward the day side. Storm I_4 developed the initial and main phases in the midnight-dawn zone at 04:00 MLT, and its recovery phase also began more on the day side. Contrasting the analyses in Table 2 and Figure 8, we notice that the observations recorded by SER agree with Li *et al.*, 2011, who researched the distribution of the H depressions with magnetic local times (MLT). They proposed that in the ring current injection that occurs during a geomagnetic storm, the particles are mostly present between dusk and midnight sectors, with drifting toward dusk, and producing a highly asymmetric geomagnetic disturbance with MLT. Then, for the storms analyzed, the partial ring current in the dusk sector is the predominant contributor to the depressions of the H component during the main phase, as the higher R values between the Dst index and H component prove during the initial and main phases of storms I_1 , I_2 , I_3 , and I_5 . Weak H variations affected storm I_4 in the dawn sector, so the storm obtains lower R values during the initial and main phases. For the recovery phase, the dawn-dusk asymmetry of the H component weakens gradually until it disappears when values return to normal.

Besides, to distinguish the action of the ionospheric currents on the selected storms, we have calculated the difference between the minimum magnitudes of Dst index (taken from WDC) and H component in SER, and the time difference at which this minimum magnitude occurs (see Table 2, columns 7 and 8, respectively). Thus, a negative (positive) $\Delta_{\text{magnitude}}$ indicates that the minimum magnitude is a little higher in SER than in the Dst index (or it is greater in the Dst than SER); and a negative (positive) Δ_{time} means that the minimum magnitude appears first in SER and afterward in the Dst index (or first in the Dst index than SER). As is shown, the storms I_1 , I_2 , I_3 , and I_5 (located from dusk till pre-dawn sectors in the night side) exhibit positive values for both differences, so they occur earlier and with greater intensity in SER than in the Dst. These results show that during the ring current injection of these storms, the ions were mostly present in the dusk and pre-midnight sectors (see examples in Li *et al.* 2011). In addition, these storms were located near the magnetotail

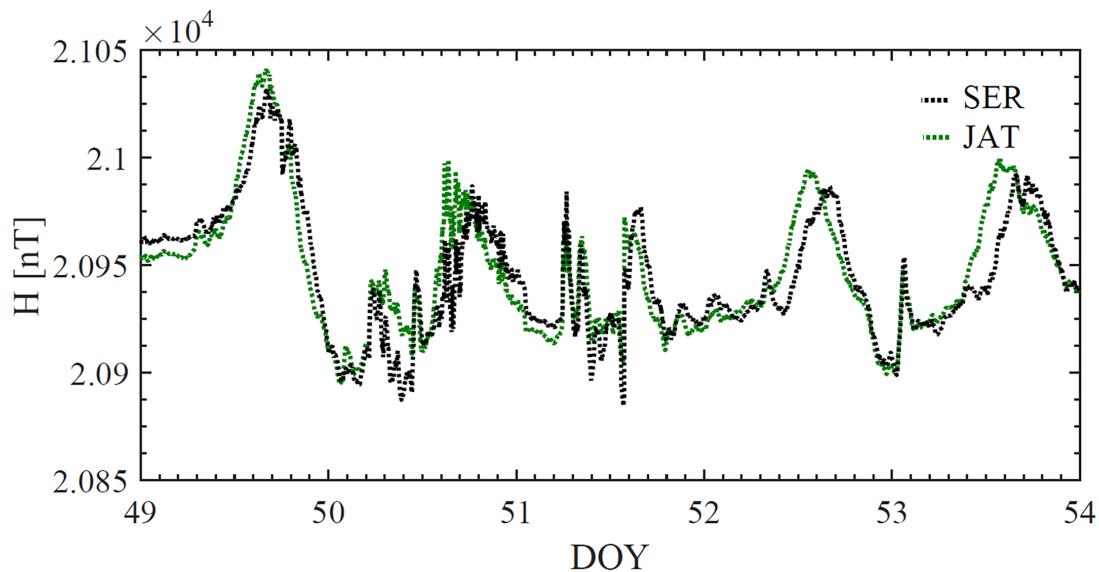


Figure 9. Comparison between the H component data recorded by SER and JAT stations (with geomagnetic latitudes of -16.55° and -12.3° , respectively) during the February 18–22, 2014, storm (I_4). JAT station is located in Brazil (17.9°S , 51.7°W) and is part of the EMBRACE array.

zone just when the electrojet was injected directly into the ring current (see examples in Martínez-Bretón *et al.*, 2016). However, only I_4 (located in the dawn sector) presents negative values in both differences so it happens earlier and with greater intensity in the Dst than SER. This fact can be influenced by a dawn current just in the transition to dayside (Martínez-Bretón *et al.*, 2016), and by the equatorial electrojet, which is very strong during the daytime (Kalegaev *et al.*, 2008). As storm I_4 shows low correlation coefficients (relative to the Dst index), we compare our data with the data recorded by Jataí station JAT, in Brazil, from EMBRACE array (Denardini *et al.*, 2018) to discard any malfunction of our instruments (see Figure 9). This analysis show correlation coefficient values of $R > 0.9$ for all phases of the storm. Note that a similar comparison was made for all storms studied, and for all cases, the correlation coefficient values were more than 0.9. In general, all our data and results are consistent with the strong influence of the magnetospheric/ionospheric current systems over the H component during an intense geomagnetic storm.

On the other hand, Häkkinen *et al.* (2003) investigated the daily and seasonal variability of the H component using time series of magnetometer data taken from official Dst stations. They demonstrated that only ~50% of this variability can be explained by three external drivers of geomagnetic activity, such as the heliographic latitude, the equinoctial effect, and the Russell–McPherron effect. Therefore, they suggested that the other 50% of the daily and seasonal variability could be explained by the distribution of the hemispheric stations. Note that the distribution is key because the hemispheric asymmetry of the geomagnetic field (that is mainly evidenced for the field minimization at the South Atlantic Magnetic Anomaly) can cause N-S amplitude differences without a specific annual pattern and randomly distributed over time (Pinto *et al.*, 1992). Thus, both the installation and management of southern magnetic ground stations such as SER according to modern standards are crucial for monitoring magnetospheric disturbances and other related phenomena.

Also, it should be noted that this work aims to show the measurements of a new geomagnetic station in the South American region and to compare their signatures concerning the global Dst index. However, it must be remembered that each local magnetic signature is unique, and the global index is obtained from the average of some of these. Saiz *et al.* (2021) showed that is possible to miss hazardous space weather disturbances using the global Dst index, and that large negative H peak recorded at any geomagnetic station might disappear in the average of the H-component from the global index observatories. Also, they proposed that the assessment of extreme events should be based on local records instead of the commonly used global indices. For this, the operation of new magnetometers for the South American region is good news to have better regional coverage of space weather events and to understand the particular characteristics of the Chilean region.

Finally, we declare that the geomagnetic field data SER recorded are consistent with the Dst index variations reported, and were obtained according to modern standards for magnetic stations. The University of La Serena's Laboratory for Space and Atmospheric Physics (LAFESAT) has developed quality infrastructure that guarantees SER's correct operation. For interested researchers, SER has recorded geomagnetic field data uninterrupted from late 2013 to now, which are available on the SAMBA website (<http://magnetometers.bc.edu/>). SER constitutes a new in situ tool of a low-latitude ground-based station that can contribute to magnetospheric research.

CONCLUSIONS

We studied five intense geomagnetic storms during the maximum phase of solar cycle 24 by using ground-level magnetic field data reported by the La Serena low-latitude magnetic ground station.

Based on the results and discussions in this study, these main conclusions obtain: (i) Due to the complexities of magnetospheric research, the installation and management of new magnetic ground stations according to modern standards is crucial. In response to development of new in situ tools and ground-based data sets that facilitate these studies, the records generated by the La Serena low-latitude magnetic ground station to describe magnetospheric disturbances and other related phenomena are available; (ii) Results evidence that H component variations measured by the La Serena station are consistent with the Dst index variations reported for each storm analyzed, obtaining correlation coefficient values of up to 0.97 for storms with $Dst < -200$ nT; (iii) The partial ring current in the dusk and night side sectors are the predominant contributor to the depressions of the H component during the main phase of the storms analyzed; (iv) Geomagnetic field values recorded by the La Serena station are useful in studies related to geomagnetic activity and reliable because the University of La Serena's Laboratory for Space and Atmospheric Physics (LAFESAT) has developed quality infrastructure that guarantees correct operation.

ACKNOWLEDGMENTS

The authors thank the support of the Direction of Research and Development of the University of La Serena (DIDULS) through projects PR22135 and PR18141, and the University of La Serena's Laboratory for Space and Atmospheric Physics (LAFESAT) by the instrumental support that enabled the preparation of this paper. Special thanks go to E. Yizengaw, E. Zesta, M. B. Moldwin and the rest of the AMBER and SAMBA team for the data.

REFERENCES

- Agee E.M., Cornett E., Gleason K., 2010, An extended solar cycle 23 with deep minimum transition to cycle 24: assessments and climatic ramifications, *J. Clim.*, 23, 6110–6114.
- Anderson D., Anghel A., Chau J., Veliz O., 2004, Daytime vertical E×B drift velocities inferred from ground-based magnetometer observations at low latitudes, *Space Weather*, 2, S11001(1)–S11001(9).
- Astafyeva E., Zakharenkova I., Förster M., 2015, Ionospheric response to the 2015 St. Patrick's Day storm: A global multi-instrumental overview, *J. Geophys. Res. Space Phys.*, 120, 9023–9037.
- Atulkar R., Bhardwaj S., Khatarkar P., Bhawre P., Purohit P.K., 2014, Geomagnetic disturbances and its impact on ionospheric critical frequency (foF2) at high, mid and low latitude región, *Am. J. Astron. Astrophys.*, 2, 61–65.
- Baker D.N., Jaynes A.N., Kanekal S.G., Foster J.C., Erickson P.J., Fennell J.F., Blake J.B., Zhao H., Li X., Elkington S.R., Henderson M.G., Reeves G.D., Spence H.E., Kletzing C.A., Wygant J.R., 2016, Highly relativistic radiation belt electron acceleration, transport, and loss: Large solar storm events of March and June 2015, *J. Geophys. Res. Space Phys.*, 121, 6647–6660.
- Bartels J., 1949, The standardized index, Ks, and the planetary index, *Kp*. *IATME Bull.*, 12b, 97–120.
- Berdichevsky D.B., Richardson I.G., Farrugia J.C., 2016, Comparative study of the December 28, 2015–January 2, 2016 and April 7–11, 1997 Sun-Earth connection events, in: 2016 AGU Fall General Assembly, id. SH13B-2300, AGU, San Francisco, CA, USA.
- Bogdanova Y., Dunlop M., Zhang Q., Perry C., Shen C., 2014, Ring Current Morphology and Properties: Statistic from Cluster, *Geophysical Research Abstracts*, 16, EGU2014-6591.
- Chen P.F., 2011, Coronal mass ejections: models and their observational basis, *Living Rev. Solar Phys.*, 8, 1–92.

- Daglis I.A., Thorne R.M., Baumjohann W., Orsini S., 1999, The Terrestrial Ring Current: Origin, Formation, and Decay, *Rev. Geophys.*, 37, 407–438.
- Denardini C.M., Chen S.S., Resende L.C.A., Moro J., Bilibio A.V., Fagundes P.R., Gende M.A., Cabrera M.A., Bolzan M.J.A., Padilha A.L., Schuch N.J., Hormaechea J.L., Alves L.R., Barbosa Neto P.F., Nogueira P.A.B., Picanço G.A.S., Bertolotto T.O., 2018, The Embrace Magnetometer Network for South America: Network description and its qualification, *Radio Sci.*, 53, 288–302.
- Doumbia V., Boka K., Kouassi N., Grodji O.D.F., Amory-Mazaudier C., Menvielle M., 2017, Induction effects of geomagnetic disturbances in the geo-electric field variations at low latitudes, *Ann. Geophys.*, 35, 39–51.
- Durgonics T., Komjathy A., Verkhoglyadova O., Shume E.B., Benzoni H.H., Mannucci A.J., Butala M.D., Høeg P., Langley R.B., 2017, Multiinstrument observations of a geomagnetic storm and its effects on the Arctic ionosphere: a case study of the 19 February 2014 storm, *Radio Sci.*, 52, 146–165.
- Eddy J.A., 1976, The Maunder minimum, *Science*, 192, 1189–1202.
- Engebretson M., Zesta E., 2017, Ground Magnetometer Array Planning: Report of a Workshop, Augsburg College, Minneapolis, MN, USA.
- Feynman J., Ruzmaikin A., 2011, The Sun's strange behavior: Maunder minimum or Gleissberg cycle?, *Sol. Phys.*, 272, 351–363.
- Ganushkina N.Y., Liemohn M.W., Dubyagin S., 2018, Current systems in the Earth's magnetosphere, *Rev. Geophys.*, 56, 309–332.
- Ghamry E., Lethy A., Arafa-Hamed T., Elaal E.A., 2016, A comprehensive analysis of the geomagnetic storms occurred during 18 February and 2 March 2014, *NRIAG J. Astron. Geophys.*, 5, 263–268.
- Goldstein J., Angelopoulos V., De Pascuale S., Funsten H.O., Kurth W.S., LLera K., McComas D.J., Perez J.D., Reeves, G.D., Spence H.E., Thaller S.A., Valek P.W., Wygant J.R., 2016, Cross-scale observations of the 2015 St. Patrick's Day storm: THEMIS, Van Allen Probes, and TWINS, *J. Geophys. Res. Space Phys.*, 121, 368–392.
- Gonzalez W.D., Joselyn J.A., Kamide Y., Kroehl H.W., Rostoker G., Tsurutani B.T., Vasyliunas V.M., 1994, What is a geomagnetic storm?, *J. Geophys. Res.*, 99, 5771–5792.
- Gopalswamy N., Xie H., Akiyama S., Makela P.A., Yashiro S., 2014, Major solar eruptions and high-energy particle events during solar cycle 24, *Earth Planet Space*, 66, 104(1)–104(15).
- Gopalswamy N., Yashiro S., Michalek G., Xie H., Lepping R.P., Howard R.A., 2005, Solar source of the largest geomagnetic storm of cycle 23, *Geophys. Res. Lett.*, 32, L12S09(1)–L12S09(5).
- Gosling J.T., McComas D.J., Phillips J.L., Bame S.J., 1991, Geomagnetic activity associated with earth passage of interplanetary shock disturbances and coronal mass ejections, *J. Geophys. Res.*, 96, 7831–7839.
- Gromova L.I., Kleimenova N.G., Levitin A.E., Gromov S.V., Dremukhina L.A., Zelinskii, N.R., 2016, Daytime geomagnetic disturbances at high latitudes during a strong magnetic storm of June 21–23, 2015: the storm initial phase, *Geomagn. Aeron.*, 56, 281–292.
- Hairston M., Coley W.R., Stoneback R., 2016, Responses in the polar and equatorial ionosphere to the March 2015 St. Patrick Day storm, *J. Geophys. Res. Space Phys.*, 121, 11213–11234.
- Hao J., Zhang M., 2011, Hemispheric helicity trend for solar cycle 24, *Astrophys. J. Lett.*, 733, L27(1)–L27(6).
- Hapgood M.A., 2011, Towards a scientific understanding of the risk from extreme space weather, *Adv. Space Res.*, 47, 2059–2072.
- Häkkinen L.V.T., Pulkkinen T.I., Pirjola R.J., Nevanlinna H., Tanskanen E.I., Turner N.E., 2003, Seasonal and diurnal variation of geomagnetic activity: revised Dst versus external drivers, *J. Geophys. Res. Space Phys.*, 108, 1060.
- Jacobsen K.S., Andalsvik Y.L., 2016, Overview of the 2015 St. Patrick's day storm and its consequences for RTK and PPP positioning in Norway, *J. Space Weather Space Clim.*, 6, A9(1)–A9(12).

- Joshi N.C., Bankoti N.S., Pande S., Pande B., Pandey K., 2011, Relationship between interplanetary field/plasma parameters with geomagnetic indices and their behavior during intense geomagnetic storms, *New Astron.*, 16, 366–385.
- Kalegaev V., Makarenkov E., 2008, Relative importance of ring and tail currents to Dst under extremely disturbed conditions, *J. Atmos. Sol.-Terr. Phys.*, 70, 519–525.
- Kalegaev V.V., Bakhmina K.Y., Alexeev I.I., Belenkaya E.S., Feldstein Y.I., Ganuskina N.V., 2008, Ring Current Asymmetry during a Magnetic Storm, *Geomagn. Aeron.*, 48, 6, 747–758.
- Kalita B.R., Hazarika R., Kakoti G., Bhuyan P.K., Chakrabarty D., Seemala G.K., Wang K., Sharma S., Yokoyama T., Supnithi P., Komolmis T., Yatini C.Y., Le Huy M., Roy P., 2016, Conjugate hemisphere ionospheric response to the St. Patrick's Day storms of 2013 and 2015 in the 100°E longitude sector, *J. Geophys. Res. Space Phys.*, 121, 1–27.
- Kamide Y., Kusano K., 2013, Is something wrong with the present solar maximum?, *Space Weather*, 11, 140–1411.
- Kamide Y., Kusano K., 2015, No major solar flares but the largest geomagnetic storm in the present solar cycle, *Space Weather*, 13, 365–367.
- Kamide Y., Richmond A.D., Matsushita S., 1981, Estimation of ionospheric electric fields, ionospheric currents, and field-aligned currents from ground magnetic records, *J. Geophys. Res.*, 86, 801–813.
- Keika K.L., Kistler L.M., Brandt P.C., 2013, Energization of O⁺ ions in the Earth's inner magnetosphere and the effects on ring current buildup: A review of previous observations and possible mechanisms, *J. Geophys. Res. Space Phys.*, 118, 7, 4441–4464.
- Le G., 2013, Magnetic Field Observations of the Ring Current in the inner Magnetosphere and Ionosphere. American Geophysical Union, Spring Meeting, abstract SM33A-01.
- Le G., Chi P.J., Strangeway R.J., Russell C.T., Slavin J.A., Takahashi K., Singer H.J., Anderson B.J., Bromund K., Fischer D., Kepko E.L., Magnes W., Nakamura R., Plaschke F., Torbert R.B., 2017, Global observations of magnetospheric high-m poloidal waves during the 22 June 2015 magnetic storm, *Geophys. Res. Lett.*, 44, 3456–3464.
- Li H., Wang C., Kan J.R., 2011, Contribution of the partial ring current to the SYMH index during magnetic storms, *J. Geophys. Res.*, 116, A11222(1)–A11222(12).
- Lingri D., Mavromichalaki H., Belov A., Eroshenko E., Yanke V., Abunin A., Abunina M., 2016, Solar activity parameters and associated Forbush decreases during the minimum between cycles 23 and 24 and the ascending phase of cycle 24, *Solar Phys.*, 291, 1025–1041.
- Liu Y.D., Hu H., Wang R., Yang Z., Zhu B., Liu Y.A., Luhmann J.G., Richardson J.D., 2015, Plasma and magnetic field characteristics of solar coronal mass ejections in relation to geomagnetic storm intensity and variability, *Astrophys. J. Lett.*, 809, L34(1)–L34(6).
- Loewe C.A., Pröls G.W., 1997, Classification and mean behavior of magnetic storms, *J. Geophys. Res.*, 102, 14209–14213.
- Love J.J., 2008, Magnetic monitoring of earth and space, *Phys. Today*, 61, 31–37.
- Love J.J., Chulliat A., 2013, An international network of magnetic observatories, *Eos Trans. AGU*, 94, 373–384.
- Love J.J., Finn C.A., 2011, The USGS Geomagnetism Program and its role in space weather monitoring, *Space Weather*, 9, S07001(1)–S07001(5).
- Love J.J., Rigler E.J., Pulkkinen A., Balch C.C., 2014, Magnetic storms and induction hazards, *Eos Trans. AGU*, 95, 445–446.
- Maltsev Y., 2004, Points of controversy in the study of magnetic storms, *Space Sci. Rev.*, 110, 227–267.
- Mandea M., Korte M., 2011, *Geomagnetic Observations and Models*, Springer, The Netherlands.
- Martínez-Bretón J.L., Mendoza Ortega B., Hernández-Quintero E., 2016, Relationship between the minima of the horizontal magnetic component measured in Mexico and the Dst and SYM-H indices for geomagnetic storms with Dst ≤ -100nT during the descending phase of solar cycle 23, *Geofis. Int.*, 55, 155–164.

- Matzka J., Chulliat A., Mandea M., Finlay C., Qamili E., 2010, Geomagnetic observations for main field studies: from ground to space, *Space Sci. Rev.*, 155, 29–64.
- Matzka J., Stolle C., Yamazaki Y., Bronkalla O., Morschhauser A., 2021, The geomagnetic Kp index and derived indices of geomagnetic activity, *Space Weather*, 19, e2020SW002641.
- Mauquoy D., Geel B., Blaauw M., Plicht J., 2002, Evidence from north-west European bogs shows ‘Little Ice Age’ climatic changes driven by variations in solar activity, *The Holocene*, 12, 1–6.
- McDonald F.B., Webber W.R., Reames D.V., 2010, Unusual time histories of galactic and anomalous cosmic rays at 1 AU over the deep solar minimum of cycle 23/24, *Geophys. Res. Lett.*, 37, L18101(1)–L18101(5).
- Nava B., Rodríguez-Zuluaga J., Alazo-Cuartas K., Kashcheyev A., Migoya-Orué Y., Radicella S. M., Amory-Mazaudier C., Fleury R., 2016, Middle- and low-latitude ionosphere response to 2015 St. Patrick’s Day geomagnetic storm, *J. Geophys. Res. Space Phys.*, 121, 3421–3438.
- Onsager T.G., 2012, Advancing space weather services through international coordination, *Space Weather*, 10, S04004(1)–S04004(4).
- Owens M.J., Lockwood M., Hawkins E., Usoskin I., Jones G.S., Barnard L., Schurer A., Fasullo J., 2017, The Maunder minimum and the Little Ice Age: an update from recent reconstructions and climate simulations, *J. Space Weather Space Clim.*, 7, A33(1)–A33(10).
- Pesnell W., 2014, Predicting solar cycle 24 using a geomagnetic precursor pair, *Sol. Phys.*, 289, 2317–2331.
- Piersanti M., Alberti T., Bemporad A., Berrilli F., Bruno R., Capparell V., Carbone V., Cesaroni C., Consolini G., Cristaldi A., Del Corpo A., Del Moro D., Di Matteo S., Ermolli I., Fineschi S., Giannattasio E., Giorgi F., Giovannelli L., Guglielmino S.L., Laurenza M., Lepreti F., Marcucci M.F., Martucci M., Mergè M., Pezzopane M., Pietropaolo E., Romano P., Sparvoli R., Spogli L., Stangalini M., Vecchio A., Vellante M., Villante U., Zuccarello F., Heilig B., Reda J., Lichtenberger J., 2017, Comprehensive analysis of the geoeffective solar event of 21 June 2015: effects on the magnetosphere, plasmasphere, and ionosphere systems, *Solar Phys.*, 292, 169(1)–169(56).
- Pinto O., Gonzalez W.D., Pinto I.R.C.A., Gonzalez A.L.C., Mendes O., 1992, The South Atlantic Magnetic Anomaly: three decades of research, *J. Atmos. Sol. Terr. Phys.*, 54, 1129–1134.
- Ray S., Roy B., Paul K.S., Goswami S., Oikonomou C., Haralambous H., Chandel B., Paul A., 2017, Study of the effect of March 17-18, 2015 geomagnetic storm on the Indian longitudes using GPS and C/NOFS, *J. Geophys. Res. Space Phys.*, 122, 2551–2563.
- Reiff P.H., Daou A.G., Sazykin S.Y., Nakamura R., Hairston M.R., Coffey V., Chandler M.O., Anderson B.J., Russell C.T., Welling D., Fuselier S.A., Genestreti K.J., 2016, Multispacecraft observations and modeling of the 22/23 June 2015 geomagnetic storm, *Geophys. Res. Lett.*, 43, 7311–7318.
- Richardson I.G., 2013, Geomagnetic activity during the rising phase of solar cycle 24, *J. Space Weather Space Clim.*, 3, A08(1)–A08(11).
- Richmond A.D., Kamide Y., 1988, Mapping electrodynamic features of the high-latitude ionosphere from localized observations: technique, *J. Geophys. Res.*, 93, 5741–5759.
- Russell C.T., Luhmann J.G., Jian L.K., 2010, How unprecedented a solar minimum?, *Rev. Geophys.*, 48, RG2004(1)–RG2004(16).
- Sainz E., Cid C., Guerreo A., 2021, The relevance of local magnetic records when using extreme space weather events as benchmarks, *J. Space Weather Space Clim.*, 11, 35(1)–35(21).
- Salinas A., Toledo-Redondo S., Navarro E.A., Fornieles-Callejón J., Portí J.A., 2016, Solar storm effects during Saint Patrick’s Days in 2013 and 2015 on the Schumann resonances measured by the ELF station at Sierra Nevada (Spain), *J. Geophys. Res. Space Phys.*, 121, 12234–12246.
- Schwabe H., 1844, Sonnen-Beobachtungen im Jahre 1843, *Astron. Nachr.*, 21, 233–236.
- Sugiura M., 1964, Hourly values of equatorial Dst for the IGY, *Ann. Int. Geophys. Year*, 35, 9–45.

- Sugiura M., Kamei T., 1991, Equatorial DST Index 1957–1986, In: Berthelier A. and Menvielle M. (Eds.), *AGA Bull. 40, Int. Serv. Geomagn. Indices Publ Off.*, Saint-Maur-des-Fosses, France.
- Tsurutani B.T., Gonzalez W.D., Tang F., Akasofu S.I., Smith E.J., 1988, Origin of interplanetary southward magnetic fields responsible for major magnetic storms near solar maximum (1978–1979), *J. Geophys. Res.*, 93, 8519–8531.
- Tsurutani B.T., Verkhoglyadova O.P., Mannucci A.J., Lakhina G.S., Huba J.D., 2012, Extreme changes in the dayside ionosphere during a Carrington-type magnetic storm, *J. Space Weather Space Clim.*, 2, A05(1) – A05(7).
- Verkhoglyadova O.P., Tsurutani B.T., Mannucci A.J., Mlynczak M.G., Hunt L.A., Paxton L.J., Komjathy A., 2016, Solar wind driving of ionosphere-thermosphere responses in three storms near St. Patrick's Day in 2012, 2013, and 2015, *J. Geophys. Res. Space Phys.*, 121, 8900–8923.
- Watari S., 2017, Geomagnetic storms of cycle 24 and their solar sources, *Earth Planet Space*, 69, 70(1)–70(8).
- Waters C.L., Gjerloev J.W., Dupont M., Barnes R.J., 2015, Global maps of ground magnetometer data, *J. Geophys. Res. Space Phys.*, 120, 9651–9660.
- Webb D.F., Howard T.A., 2012, Coronal mass ejections: observations, *Living Rev. Solar Phys.*, 9, 1–83.
- Welling D.T., Jordanova V.F., Zaharia G., 2011, The effects of dynamic ionospheric outflow on the ring current. *J. Geophys. Res.*, 116, A00J19.
- White O., Kopp G., Snow M., Tapping K., 2011, The solar cycle 23–24 minimum. A benchmark in solar variability and effects in the heliosphere, *Solar Phys.*, 274, 159–162.
- Williams P.E., Pesnell W.D., 2011, Comparisons of supergranule characteristics during the solar minima of cycles 22/23 and 23/24, *Solar Phys.*, 270, 125–136.
- Wu C.C., Liou K., Lepping R.P., Hutting L., Plunkett S., Howard R.A., Socker D., 2016, The first super geomagnetic storm of solar cycle 24: “The St. Patrick's day event (17 March 2015)”, *Earth Planet Space*, 68, 151(1)–151(12).
- Yao Y., Liu L., Kong J., Zhai C., 2016, Analysis of the global ionospheric disturbances of the March 2015 great storm, *J. Geophys. Res. Space Phys.*, 121, 12157–12170.
- Yizengaw E., Moldwin M.B., Zesta E., Biouele C.M., Damtie B., Mebrahtu A., Rabiou B., Valladares C.F., Stoneback R.A., 2014, The longitudinal variability of equatorial electrojet and vertical drift velocity in the African and American sectors, *Ann. Geophys.*, 32, 231–238.
- Zakharenkova I., Astafyeva E., Cherniak I., 2015, Early morning irregularities detected with spaceborne GPS measurements in the topside ionosphere: A multisatellite case study, *J. Geophys. Res. Space Phys.*, 120, 8817–8834.
- Zakharenkova I., Astafyeva E., Cherniak I., 2016, GPS and GLONASS observations of large-scale traveling ionospheric disturbances during the 2015 St. Patrick's Day storm, *J. Geophys. Res. Space Phys.*, 121, 12138–12156.
- Zolotukhina N., Polekh N., Kurkin V., Rogov D., Romanova E., Chelpanov M., 2017, Ionospheric effects of St. Patrick's storm over Asian Russia: 17–19 March 2015, *J. Geophys. Res. Space Phys.*, 122, 2484–2504.